Proceedings of ASME Turbo Expo 2020
Turbomachinery Technical Conference and Exposition
GT2020
June 22-26, 2020, London, England

GT2020-14953

EMISSIONS PERFORMANCE OF STAGED PREMIXED AND DIFFUSION COMBUSTOR CONCEPTS FOR AN NH_3/AIR FLAME WITH AND WITHOUT REACTANT HUMIDIFICATION

D. Pugh, A. Valera-Medina, P. Bowen, A. Giles, B. Goktepe
J. Runyon, S. Morris, S. Hewlett, R. Marsh,

Cardiff University School of Engineering,
Cardiff, Wales, UK, CF24 3AA.
Email: pughdg@cardiff.ac.uk

ABSTRACT

Renewably generated ammonia offers a form of carbon-free chemical energy storage to meet the differences between uncertain supply and fluctuating demand and has the potential to support future energy requirements. The storage/transportation characteristics of NH_3 are favorable compared with H_2, however there are combustion research challenges to enhance fuel reactivity whilst reducing harmful emissions production. The purpose of this work was to evaluate different fuel delivery concepts for a representative GT combustor. An experimental and numerical comparison was made between swirl-stabilized premixed and diffusion NH_3-air flames at elevated inlet temperature (473 K). The exhaust NOx and NH_3 emissions generated from each concept were quantified to optimize combustor performance. High-speed OH and NH_2* chemiluminescence was employed to characterize the change in flame topology with variation in fuel-air equivalence ratio, and the resultant influence on measured emission concentrations. Chemiluminescence intensities were shown to elucidate changes in sampled exhaust emissions, enabling detailed analysis of intermediate chemistry. A comparison was made between experimental data and kinetic simulations, demonstrating the sensitivity of NO_x emissions to premixed fuel-air equivalence ratio. A comparison was also made between exclusive primary airflow, and the staged introduction of secondary air, to quantify the change in NO_x production between each configuration and improve fuel burnout. Secondary air loadings were incrementally increased through the combustor. Finally, reactant humidification was employed as a secondary process for NO_x reduction, having shown favorable performance with NH_3-H_2 mixtures, with the efficacy compared for both premixed and diffusion configurations.*

Keywords: Ammonia, staged combustion, NO_x emissions, humidification, chemical kinetics modelling.

NOMENCLATURE

AFT	Adiabatic Flame Temperature (K)
CRN	Chemical Reactor Network
CRZ	Central Recirculation Zone
FZ	Flame Zone
ORZ	Outer Recirculation Zone
P	Pressure (MPa)
PFR	Plug Flow Reactor
Re	Reynolds Number
SA	Secondary Air
S_g	Geometric swirl number
S_L	Laminar Flame speed ($cm \cdot s^{-1}$)
T	Temperature (K)
WL	Water Loading ($g \cdot s^{-1}$)
Φ	Equivalence Ratio
Φ_G	Global Equivalence Ratio

1. INTRODUCTION

There is increasing interest in using renewably generated NH_3 (sometimes termed 'green ammonia') as a prospective energy carrier [1,2] and a mechanism for storing H_2. Green H_2 is produced via the electrolysis of water using renewable electricity, and in-turn green ammonia is manufactured using green H_2 and nitrogen. With existing infrastructure and favorable storage/transportation characteristics, the potential exists to supply power systems with NH_3, avoiding conversion back to H_2. However, this presents several combustion research challenges [2-6]: NH_3 reactivity is poor compared to traditional hydrocarbon fuels, with peak laminar flame speeds (S_L) at atmospheric conditions ~8 $cm{\cdot}s^{-1}$. Combustion performance can be enhanced by thermolysis to form H_2 [7-9], preheating, or supplementary fuel blending [8-12]. A more significant challenge is the propensity for excessive exhaust NO_x concentrations from fuel-bound nitrogen [12-15]. Conventionally employed lean, low-temperature combustor strategies are ineffective for NO_x reduction with NH_3/air flames, with previous studies demonstrating concepts such as humidification [3] and staging [14-15] more successful, alongside an increase in combustor pressure [3,16-17]. This makes the prospective application of NH_3 for energy conversion more favorable for gas turbines.

1.1 Scope of This Work

Contemporary research is mostly directed towards the development of low-NO_x NH_3 combustors [3,14,17], exploring staged concepts, and comparing performance against CH_4-air flames [15,18]. Through the optimized introduction of staged secondary-air, pathways have been identified that limit NO_x production in a fuel-rich primary flame, whilst improving combustor efficiency through reducing unburned NH_3 and H_2 [3,14,17,18]. However, the number of detailed experimental studies with NH_3 flames remains limited, particularly at elevated inlet conditions, and an optimized flame configuration that provides both low NO_x and NH_3 will greatly impact the performance of downstream staging. Recent work undertaken by the authors has focused on H_2 blending strategies [5], and changes in combustor pressure [3]. However, the purpose of this study was to expand on recent findings to investigate the change in emissions from a pure NH_3/air flame, exploring NO reduction pathways through the detailed numerical and experimental investigation of distinct mechanisms of fuel delivery. A fuel-flexible generic swirl burner was employed in both premixed and diffusion configurations with swirl-stabilized NH_3-air flames. Regions of excited OH* and NH_2* were visualized in the primary flame using Abel transformed high-speed chemiluminescence and compared against emissions produced. Changes in secondary air loading and reactant humidification were subsequently made to quantify any resultant variation in total emissions production.

2. EXPERIMENTAL CONDITIONS

Initial experiments were undertaken using NH_3-air mixtures with a fully premixed flame configuration, achieved by directing all reactants to the outer swirling flow (flow-path 2 - Fig.1). The fuel supply was then withdrawn for the non-premixed experiments, with NH_3 instead directed to the central diffusion jet (flow-path 1 - Fig.1). Data points were specified for primary equivalence ratios in the range Φ=0.9-1.2 by varying the swirling air flow rate. Ambient combustor inlet conditions of temperature (T) and pressure (P) were held constant at respective values of 473±5 K and 0.11 ±0.005 MPa. With the fully premixed configuration, swirler nozzle bulk outlet velocities were varied from ~9-11 $m{\cdot}s^{-1}$ across the specified Φ range with Reynolds numbers increasing from Re=~10,700 to ~13,400 at the highest flow conditions. These values were reduced by approximately 20% for the diffusion case. Initially, data were captured from only the primary flame (SA_0), with secondary airflow then increased at two fixed mass loadings: 3 $g{\cdot}s^{-1}$ (SA_1) and 6 $g{\cdot}s^{-1}$ (SA_2). These flow rates correspond to approximately 50 and 100% of primary airflow at the richest condition. Finally, humidification of the reactant airflow was appraised, having previously shown to be effective in reducing exhaust NO_x concentrations with an NH_3/H_2 flame [3]. Limited steam flow rates could be achieved before the flame became unstable – realised by intermittent detachment from the burner nozzle – with data captured for a constant water loading of 0.2 $g{\cdot}s^{-1}$ (WL_1) at Φ=1, corresponding to ~3%$_{vol}$ of the total reactant composition, or ~5%$_{vol}$ of the airflow. Fuel flow was maintained at a constant mass flow rate of 1.34 $g{\cdot}s^{-1}$ for all conditions, to give a net thermal power of 25 kW_{th}. The experimental conditions and flowrates are summarized in Table 1.

TABLE 1: SUMMARY OF EXPERIMENTAL CONDITIONS

Φ	**Fuel Flow** ($g{\cdot}s^{-1}$)	**Air Flow** ($g{\cdot}s^{-1}$)	**SA** ($g{\cdot}s^{-1}$)	**WL** ($g{\cdot}s^{-1}$)
0.9	1.34	9.04	0, 3, 6	0
1		8.13		0, 0.2
1.1		7.39		0
1.2		6.78		0

3. EXPERIMENTAL FACILITY

The employed swirl burner is presented as a cross-sectional schematic in Fig.1, with a central diffusion lance (Fig.1a) added to facilitate the introduction of a jet to the annular swirling flow. The lance ID (15 mm) was specified to generate approximately equal jet velocities (flow-path 1 in Fig. 1) to the outer flow (flow-path 2) at the highest airflow condition. For the premixed configuration, reactants were mixed prior to entering the inlet plenum (Fig.1b) with flows metered using Coriolis mass-flow control (±0.35%). The plenum body was preconditioned to 473K using electric preheaters and compressed air, dried to a dew point of -17°C. System temperatures were allowed to stabilize for at

least an hour before experiments began. From the premix chamber (Fig.1c), reactants flow through a radial-tangential swirler (Fig.1d) with a geometric swirl number of S_g=0.8 and out the exit nozzle (r=20mm). Quartz windows (Fig.1e) provided optical access into the pressure casing (Fig.1g) used to enclose the secondary airflow which was introduced through a single inlet (flow-path 3 - Fig.1). For humidified experiments, water supply was regulated using another scaled mass-flow controller (±0.2%) and vaporized in heaters prior to entering the preheated air stream. Chemiluminescence measurements were taken perpendicular to the reactant flow direction through the optical windows, specified to give enhanced UV transmission. The primary flame was housed within a cylindrical quartz confinement tube (Fig.1f) at an expansion ratio of 2.5 from the nozzle. Combustor pressure was controlled using a water-cooled back-pressure valve with incremental control. Greater detail of the facility can be found in other publications [19-20].

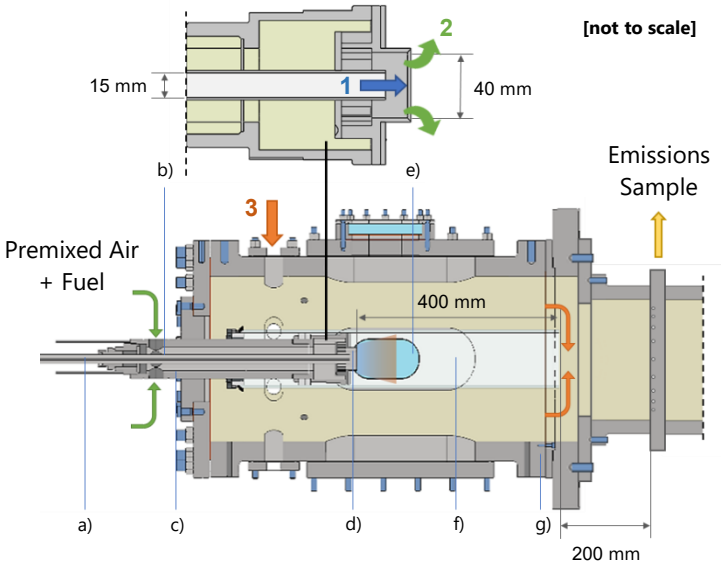

FIGURE 1: CROSS-SECTIONAL SCHEMATIC OF BURNER, CASING ASSEMBLY AND SAMPLE PROBE (LABELS

3.1 Emissions

Exhaust gas emissions were sampled downstream of the quartz confinement and secondary air mixing zone using a 9-hole equal-area probe, water-conditioned with a heat exchanger to regulate sample temperature (433K) following specifications in ISO-11042 [21]. The pump, filter block and sample lines were also maintained at the same temperature. Total NO_x (NO and NO_2) concentrations were quantified using heated vacuum chemiluminescence as the measurement technique (Signal 4000VM). NH_3 measurements were made using the same analyzer and redirecting sample through a NO converter (Signal 410) to measure unreacted concentrations (81% conversion efficiency). All NH_3 and NO_x concentrations were measured hot/wet and normalized to equivalent dry conditions using equation (9) in ISO-11042. Dry O_2 measurements were made using a paramagnetic analyzer (Signal 9000MGA) and used to subsequently normalize NO_x/NH_3 readings to 15% O_2 equivalent (equation (10) in ISO-11042). At each experimental condition, burner temperatures, pressures, flows and emissions were monitored and, once stable, held for a minimum of 60 samples to be taken. Systematic uncertainties in the analyzer (linearisation and span gas certification), were combined with any fluctuations in measurement to give the total uncertainty represented by the plotted error bars.

3.2 Chemiluminescence

Chemiluminescence measurements were obtained at each experimental condition, targeting electronically excited intermediate chemical radicals within the NH_3-air air flames. The species investigated were OH* and NH_2*, captured using a combination of Phantom v1212 high-speed CMOS camera, Specialised Imaging SIL40HG50 high-speed image intensifier, UV lens (78 mm, f/11), and narrow bandpass filters selected specifically for each species (further information on this facility is found in other works [22]). OH* chemiluminescence images were taken focusing specifically on the well-known $A^2\Sigma^+$–$X^2\Pi$ OH* system [23] using a 315 nm (±15 nm FWHM) bandpass filter. Few experimental studies have conducted NH_2* chemiluminescence measurements, and these have typically been confined to canonical reactors [24-27] or shock tubes [28-29] rather than NH_3 flames, where NH_2 and NH intermediate chemistry is key to NH_3 oxidation [1-3]. For NH_2* measurements, a single peak of the NH_3 α band was selected at 630 nm [23,26] using a bandpass filter centered at 632 nm (±10 nm FWHM). Images were captured at 4000 Hz, with the image intensifier gated at 10 μs and the intensifier gain held constant throughout. The image resolution is 4.6 pixels/mm, resulting in a field of view of 75 mm (axial, y) by 100 mm (radial, x) relative to the edge and centerline of the burner exit nozzle, respectively (Fig. 2). Each instantaneous chemiluminescence image was filtered using a 3x3 median filter and temporally averaged from 2000 images (t = 0.5 s). The resultant image was then background corrected and transformed using a modified Abel inversion algorithm. This provided an axisymmetric planar representation of the electronically-excited radical species distribution within the swirling flow field [30]. A comparison is shown between the averaged raw NH_2* chemiluminescence (Fig. 2a) and equivalent Abel transform (Fig. 2b) for an example case in Fig. 2 where the centerline of the burner nozzle is represented by x= 50mm and flow enters from the bottom.

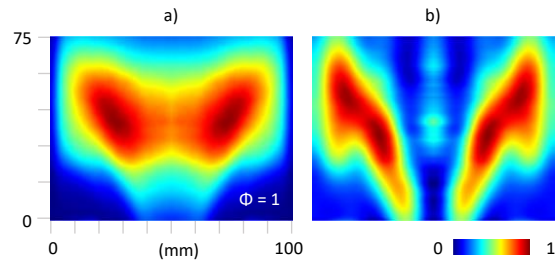

FIGURE 2: COMPARISON BETWEEN TEMPORALLY AVERAGED RAW NH_2* CHEMILUMINESCENCE (a) AND EQUIVALENT ABEL TRANSFORM (b) FOR A SAMPLE PREMIXED FLAME.

4. CHEMICAL REACTOR NETWORK MODELING

The chemical kinetics of the premixed experimental burner were simulated using Chemkin-Pro. PREMIX was employed with the laminar flame speed calculator to model changes in S_L with Φ. Solutions were based on an adaptive grid of 1000 points, with multi-component transport properties. The equilibrium reactor was used to generate adiabatic flame temperatures (AFT) under conditions of constant enthalpy/pressure. The NH_3 flame model employed the Okafor et al. reaction mechanism, optimized for use with CH_4/NH_3-air mixtures [18] with 59 chemical species and 356 reactions. The predicted changes in S_L (solid) and AFT (dashed) are shown for the range of experimental Φ in Fig. 3. A comparison is shown between the dry case at WL_0, and the humidified condition WL_1, alongside a CH4-air flame at equivalent conditions (GRI mechanism [30], 53 species and 325 reactions). The limited water loading employed in this study was shown to provide a ~12% reduction in NH_3-air S_L across the specified Φ range, with both results markedly lower than the equivalent CH4-air flame. As speeds were already low for the NH_3-air flame, water addition provided a significant drop in reactivity, leading to blow off instabilities when humidified fractions were further increased. AFT was shown to be high enough to facilitate thermal NO_x formation for the NH3-air flame and was reduced by ~50K at WL_1.

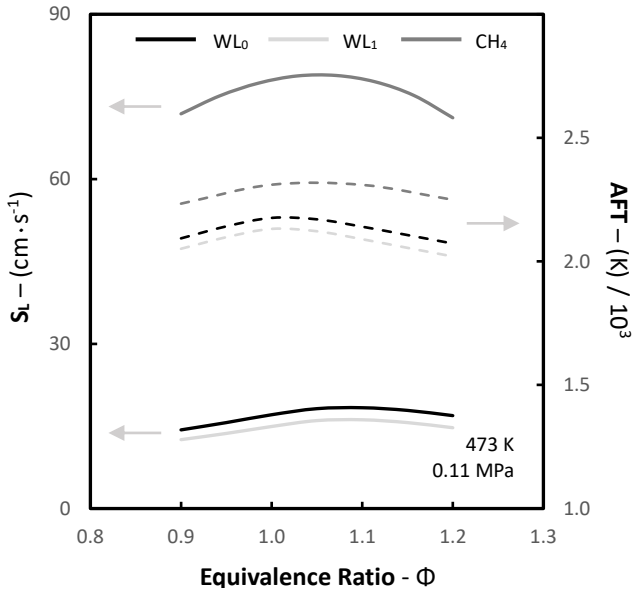

FIGURE 3: COMPARSION BETWEEN S_L (SOLID) AND AFT (DASHED) FOR THE PREMIXED NH_3-AIR, AND CH_4-AIR FLAMES AT THE SPECIFIED EXPERIMENTAL CONDITIONS.

A chemical reactor network (CRN) model was also developed to simulate the chemistry of the experimental swirling NH_3-air flame [10-11, 24], analogous to the simulation previously presented by the authors [3]. Inlets were used to provide fuel/air/steam flows, with three perfectly stirred reactors (PSR) to model the pre-mixing, flame and central recirculation zones (CRZ) (20% recycled flow [25]). The outlet from the flame zone (FZ) fed a Plug Flow Reactor (PFR) to simulate reactions in the post-flame zone. The model structure is outlined in Fig. 4 and was established with representative combustor geometry and residence times calculated from empirical flow conditions. Initial reactor temperatures were defined from equilibrium calculations. Heat loss was estimated to be 10%, with initial values compared to empirical results at dry conditions to give favorable agreement with sampled concentrations. It should be emphasized that moderate uncertainty is associated with CRN modelling, and the system developed was primarily used for qualitative analysis of trends, rather than detailed prediction.

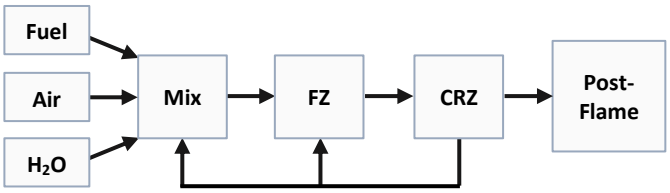

FIGURE 4: CHEMICAL REACTOR NETWORK MODEL STRUCTURE

5. RESULTS

5.1 Premixed Flame

Measured NO (empty) and NH_3 (shaded) emissions from the fully premixed flame configuration are shown plotted against Φ in Fig. 5 – data are provided for SA_0/WL_0 only. The markers show the averaged experimental data normalized to dry 15% O_2 conditions, with results from the reactor network model represented by the lines. Measured NO_2 fractions were negligible, with substantial concentrations only measured at Φ=0.9 (<40ppmvd). Overall, favorable agreement is shown in trends between the sampled and modelled results. The model

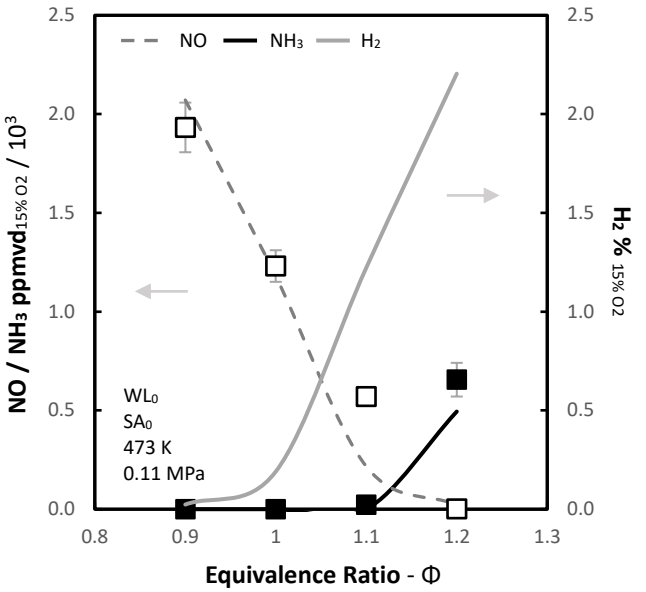

FIGURE 5: MEASURED AND MODELLED NO (EMPTY) AND NH_3 (SHADED) EMISSIONS FOR THE PREMIXED NH_3-AIR FLAME, ALONGSIDE SIMULATED H_2 CONCENTRATIONS.

also allows for the simulation of exhaust H_2 concentrations, which were not measured and are shown to rise sharply above Φ=1. This demonstrates that most of the fuel-bound nitrogen is liberated in the primary flame zone, and unreacted fuel is largely formed as H_2. Therefore, fuel-NO_x production will be limited in the secondary flame zones, though NH_3 concentrations appear to rise around Φ=1.1.

A pronounced decrease in NO with increasing Φ is also evident in Fig. 5. This results from reduced thermal formation with the Zel'dovich mechanism, with diminished availability of OH for NH_3 oxidation [16,18] and combination with HNO [3,5], alongside enhanced NO consumption with NH_2 through the chain carrying reaction $NH_2+NO \leftrightarrow NNH+OH$, and the terminating reaction $NH_2+NO \leftrightarrow H_2O+N_2$ [3]. Figure 6 shows the change in OH* and NH_2* Abel transformed chemiluminescence profiles with change in Φ. Half of the axisymmetric flame is shown, with x=0 mm corresponding to the burner nozzle centerline and flow from the bottom. The colormaps in these images have been normalized to the maximum for each species dataset to emphasize the change in reactive intensity. A complementary trend is evident for change in Φ between the reduction of OH* intensity, an increase in NH_2*, and a drop in measured exhaust NO concentrations. Using OH* as a generalized marker for heat release [23], the flame structure appears typical for a swirling premixed configuration [22,31], with the flame stabilized around a conical shear layer of zero axial velocity, with central and outer recirculation zones (CRZ and ORZ respectively). There appears to be increased reacting flow in the ORZ – giving a characteristic 'M' flame, compared to the 'V' observed for near equivalent CH_4/air flames with this burner [31].

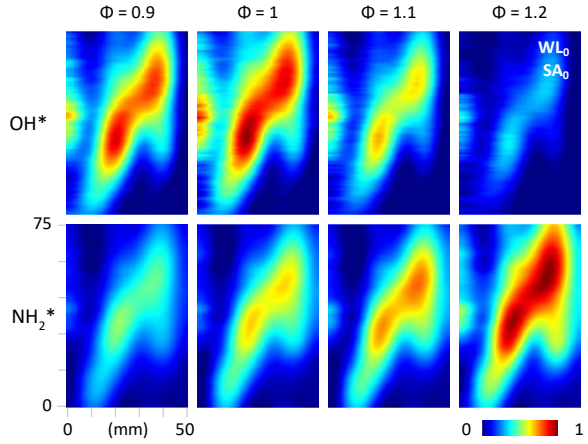

FIGURE 6: ABEL TRANSFORMED OH* AND NH_2* CHEMILUMINESCENCE FOR THE PREMIXED NH_3-AIR FLAME AND INCREASING Φ (COLORMAP NORMALIZED TO SPECIES DATASET MAXIMUM).

5.2 Diffusion Flame

A comparison between measured emission concentrations from the diffusion and premixed configurations is presented in Fig. 7 – again data are shown for SA_0/WL_0 with change in Φ. Lines are this time included for clarity as rather than presenting modelled data. There is a marked difference between the two cases, particularly at the leanest Φ, with the diffusion flame generating significantly lower NO concentrations – once again

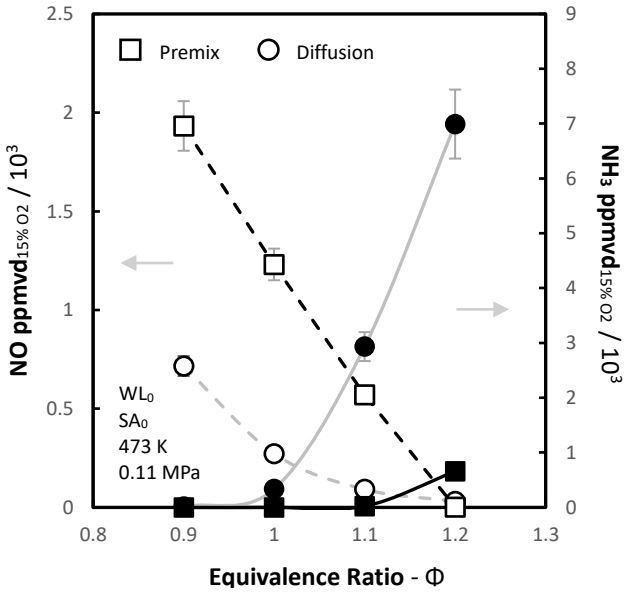

FIGURE 7: MEASURED NO (DASHED LINE) AND NH_3 (SOLID LINE) EMISSIONS FOR PREMIXED AND DIFFUSION NH_3-AIR FLAMES.

NO_2 was measured to be negligible aside from Φ=0.9, with values similar to the premixed case. Local NH_3-rich zones lead to the increased production of reactive NH_2* within the diffusion flame as observed in the NH_2* chemiluminescence shown in Fig. 8. Once again this suggests reactive NH_2 acts to consume NO through the kinetics discussed for the premixed case, with the more dispersed region of NH_2^* leading to a drop in measured NO emission concentrations.

The colormaps in Fig. 8 are this time normalized to the maximum intensity in each image to emphasize the change in flame topology with Φ. A comparison is shown between the raw averaged chemiluminescence (Fig 8b), and equivalent Abel transform (Fig 8c) - As bulk flow is decreased with increasing Φ, the effective swirl reduces and the flame appears to contract towards the centerline diminishing the influence of the CRZ, and extending beyond the observable window. Instantaneous images of measured NH_2* intensities are also included in Fig. 8a (captured at intervals of ~0.05s) to highlight the transient structure of the diffusion flame (Φ =1) employed and more dispersed regions of reacting flow, facilitated through the use of the high-speed chemiluminescence.

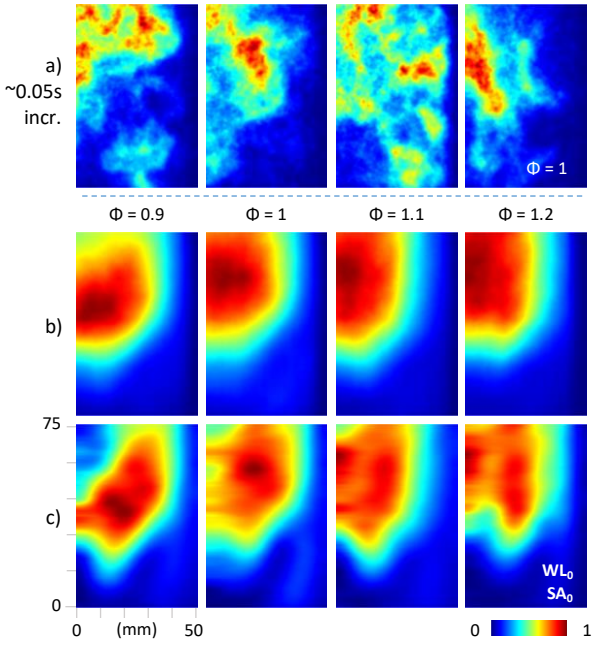

FIGURE 8: INSTANTANEOUS (a), AVERAGED RAW (b), AND ABEL TRANSFORMED (c) NH_2* CHEMILUMINESCENCE FOR THE DIFFUSION NH_3-AIR FLAME (COLORMAP NORMALIZED TO IMAGE MAXIMUM).

Whilst the diffusion flame provides the advantage of lower exhaust NO_x concentrations, combustor efficiency appears comparatively poor, with significantly higher unreacted NH_3 fractions observed in Fig. 7. Measured concentrations are shown to rise with increasing Φ to provide an order of magnitude difference between the two flame configurations. This primarily results from the elevated NH_2 concentrations observed in Fig. 8, with the respective chain branching and third body reactions $2NH_2 \leftrightarrow NH_3+NH$ and $NH_2+H+M \leftrightarrow NH_3+M$ [3]. Fuel-bound nitrogen in the excessive NH_3 emissions from the primary flame would therefore be expected to increase aggregate NO_x production with the introduction of staged secondary air to improve combustor efficiency.

5.3 Secondary Air Introduction

Secondary air was introduced to the combustor at two constant mass loadings: 3 $g \cdot s^{-1}$ - SA_1, and 6 $g \cdot s^{-1}$ - SA_2. The change in global fuel-air equivalence ratio (Φ_G) was calculated by adding the secondary air component to the primary loading, providing a range of globally lean experimental points. A comparison between the emissions produced from the diffusion and premixed flame configurations at SA_1 is shown in Fig. 9 (once again lines are included for clarity and do not represent modelled data). Emissions from the Φ_G=0.67 (corresponding to a primary Φ=0.9) case appear to provide similar measured concentrations to the equivalent SA_0 experiment – as may be expected from a lean primary flame with minimal unburned fuel concentrations. However, once the primary Φ is increased above stoichiometric, there is an offset between the measured concentrations for SA_1 and those presented in Fig 7. Unreacted H_2 and NH_3 are consumed in the secondary flame zone to produce more NO_x. The order of magnitude difference in NH_3 concentrations from the primary diffusion case lead to a crossover at Φ_G=0.83, with higher NO values than the equivalent premixed condition. Here the optimal configuration is identified with both NO and NH_3 <75ppmvd. The method of secondary air

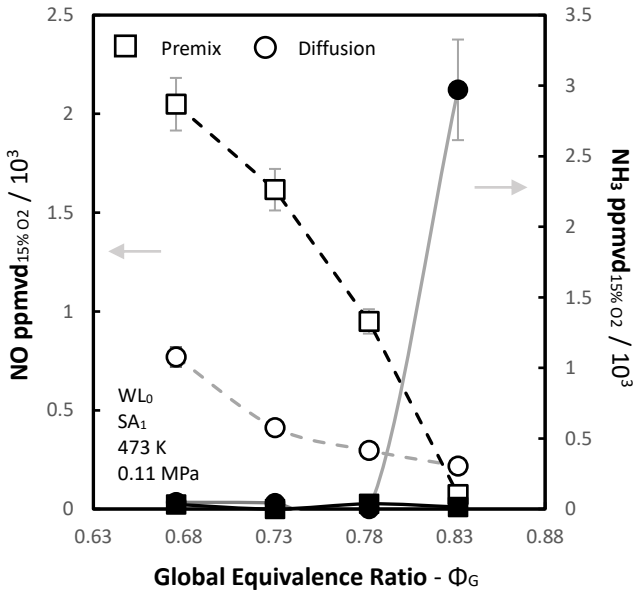

FIGURE 9: MEASURED NO (DASHED LINE) AND NH_3 (SOLID LINE) EMISSIONS FOR PREMIXED AND DIFFUSION NH_3-AIR FLAMES WITH SECONDARY AIR LOADING (SA_1).

introduction employed in this study is simple with comparatively poor mixing. This leads to inefficiency for the diffusion case, with significant unreacted NH_3 concentrations still measured at the richest condition and combustion reactions quenched in the emissions sample probe.

With the NH_3-air flame so sensitive to change in Φ, it was essential to ensure the quartz confinement tube remained effectively sealed at the premix chamber (Fig 1c), with no secondary air entrainment into the primary flame-zone. Measured chemiluminescence intensities were used to validate the employed experimental setup. Figure 10 provides a comparison of the NH_2* chemiluminescence for an example premixed case – colormaps have been normalized to the maximum intensity measured across the 4-image dataset. A marked difference is observed between the Φ=0.9 and 1 SA_0 images, with the maximum intensities around 29% higher in the latter. Whereas the respective differences observed for SA_1 and SA_2 cases were 2.4 and 0.7%, and hence the images appear near-identical in Fig. 10.

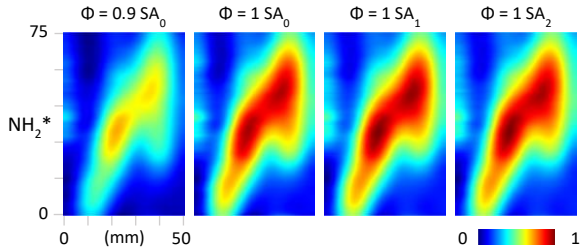

FIGURE 10: ABEL TRANSFORMED NH_2* CHEMILUMINESCENCE FOR PREMIXED NH_3-AIR FLAMES WITH SECONDARY AIR LOADING (COLORMAP NORMALIZED TO DATASET MAXIMUM).

Secondary air loading was increased further to SA_2, with the emissions dataset for the ostensibly optimal Φ=1.2 plotted against air loading in Fig. 11. For the diffusion case, as combustor efficiency is increased with enhanced air loading, more NH_3 is consumed in the secondary zone leading to higher NO concentrations, with some unburned fuel remaining in the product sample. A marginal increase in NO was observed for the premixed flame from SA_1 to SA_2 possibly resulting from enhanced H_2 consumption, or greater O_2 concentrations facilitating more NO production through OH and HNO pathways, such as HNO+OH↔NO+H_2O. NO_2 fractions were also shown to rise with an increase in secondary air loading; for low secondary air cases, negligible concentrations were measured for either flame configuration at Φ=1.2. However, once secondary air loading was increased further to SA_2, premixed and diffusion primary flames gave respective measured NO_2 concentrations of ~10 and ~100 ppmvd. Again, this results from greater O_2 availability in the secondary flame-zone, with models suggesting enhanced third body production with NO through NO+O+M↔NO_2+M. The results therefore suggest that whilst combustor efficiency can be increased through the introduction of secondary air, the dilution must be carefully controlled, as the excessive introduction of air may lead to greater NO_x production. Trials undertaken with CH_4-air mixtures in a similar burner configuration demonstrated an opposing trend [32]. Limited NO_x sensitivity to primary flame equivalence ratio was observed as a function of thermal production, with the NH_3-air flame studied here shown to be more responsive. Increased secondary air loading was also shown to reduce NO_x production, compared to the increase observed here.

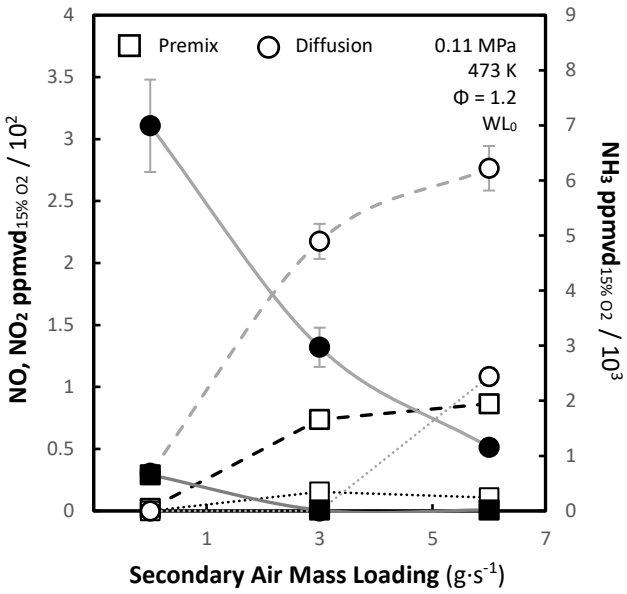

FIGURE 11: MEASURED NO (DASHED LINE), NO_2 (DOTTED LINE) AND NH_3 (SOLID LINE) EMISSIONS FOR PREMIXED AND DIFFUSION NH_3-AIR FLAMES WITH INCREASED SECONDARY AIR LOADING AT Φ=1.2

5.4 Reactant Humidification

Humidification has previously been shown by the authors to be an effective mechanism for NO_x reduction in NH_3/H_2 flames, dropping concentrations by an order of magnitude for reactant loadings of ~10% [3]. However, as discussed in previous sections, only limited steam loading could be achieved with the NH_3-air flame at 473K, before reactivity was diminished to the point of instability with intermittent extinction, or detachment from the burner nozzle. Whilst S_L is shown to drop by 12% in Fig. 3, peak heat release rate is shown to reduce by ~25% from WL_0 to WL_1. It is therefore unsurprising that increasing water loading beyond this limited value leads to extinction. Nevertheless, the change in emissions production was quantified for the specified loading at Φ=1 with the results presented in Fig. 12 for both the premixed and diffusion cases. There is an observed decrease in NO emissions with water loading for the premixed case, however this is small for the limited amount of H_2O introduced when compared with the efficacy for NH_3/H_2 mixtures. From CRN modelling, this reduction is simulated to

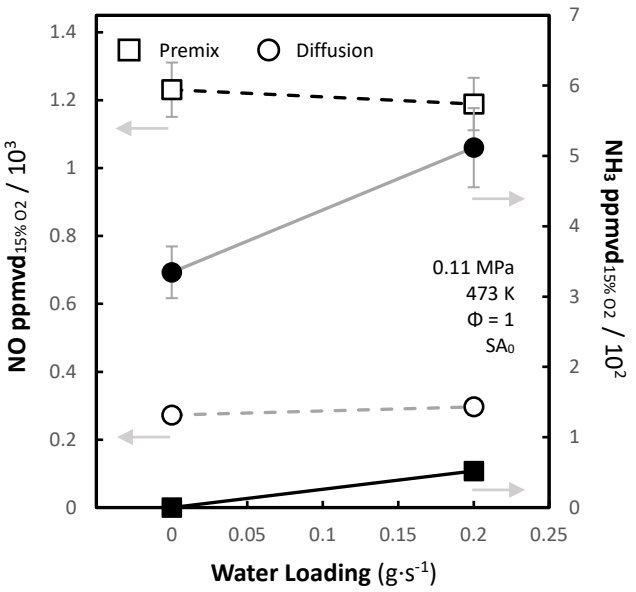

FIGURE 12: MEASURED NO (DASHED LINE) AND NH_3 (SOLID LINE) EMISSIONS FOR PREMIXED AND DIFFUSION NH_3-AIR FLAMES WITH INCREASED WATER LOADING AT Φ=1.2

result from enhanced NH_2 consumption pathways 1) $NH_2+NO \leftrightarrow NNH+OH$, and 2) $NH_2+NO \leftrightarrow H_2O+N_2$, alongside a drop in thermal NO production. Figure 13 presents a comparison of the NH_2* chemiluminescence for the premixed case at different water loadings, with colormaps again normalized to image maximum to emphasize the change in topology. The influence of H_2O is subtle, but a marginal extension of the flame brush is observed, as would be expected from reduced reactivity, and indicates a larger region of NH_2*. For the diffusion case, minimal impact was observed with NO values marginally increasing, however this change is within the measured

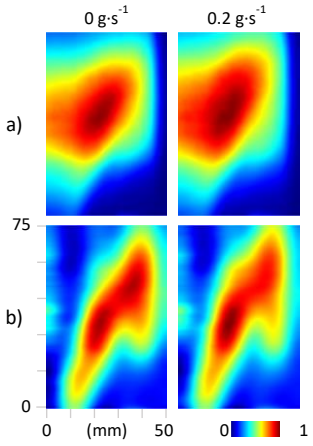

FIGURE 13: AVERAGED RAW (a) AND ABEL TRANSFORMED (b) NH_2* CHEMILUMINESCENCE FOR PREMIXED NH_3-AIR FLAMES AT Φ=1, WITH INCREASED WATER LOADING (COLORMAP NORMALIZED TO IMAGE MAXIMUM).

uncertainty of the experimental data. A rise in unreacted NH_3 was observed for both flame configurations, modelled to result from increased NH_2 production and could enhance NO_x production with downstream staging. The results therefore suggest the suitability of humidification for NO_x reduction is diminished for NH_3-air flames compared to NH_3/H_2 mixtures.

6. CONCLUSIONS

An experimental and numerical comparison was made between swirl stabilized premixed and diffusion NH_3-air flames at elevated inlet temperature (473 K). High-speed OH* and NH_2* chemiluminescence was employed to characterize the change in flame topology with variation in fuel-air equivalence ratio, and the resultant influence on measured emission concentrations. Chemiluminescence intensities were shown to elucidate changes in sampled exhaust emissions, enabling detailed analysis of intermediate chemistry.

Markedly different results were obtained for each primary flame configuration, with the diffusion case offering substantially lower measured NO concentrations at leaner conditions. The premixed flame gave more favorable emissions once an equivalence ratio of 1.2 was reached. The premixed flame also provided greater combustion efficiency, with NH_3 concentrations approximately an order of magnitude lower than each equivalent diffusion case, and unreacted fuel primarily formed as H_2. Favorable agreement was observed between experimental results, and data obtained from empirical chemical reactor network modelling. This facilitated the detailed chemical analysis of emissions formation.

The burner was subsequently employed in a staged configuration, with the incremental introduction of secondary air to increase combustor efficiency and reduce unburned fuel. Again, at the leanest global equivalence ratios, the diffusion flame provided superior emissions performance. However, for the richest experimental condition, the premixed primary flame provided NO and NH_3 concentrations <75 ppmvd. This resulted from a combination of low NO production in the primary flame and reduced fuel-bound nitrogen in the secondary reaction zone. The amount of secondary air loading must be carefully controlled however, as excessive oxygen can lead to the enhanced production of both NO and NO_2.

The efficacy of reactant humidification for NO_x reduction was also appraised for the NH_3-air flame, having shown favorable performance with NH_3/H_2 mixtures. Limited H_2O concentrations could be achieved (3%$_{vol}$ of reactant composition) with the stable flame at the specified inlet temperature, before the drop in mixture reactivity led to blow off and extinction instabilities. A reduction in NO with H_2O increase was observed for the premixed case, however both flame configurations provided an increase in exhaust NH_3, which could lead to greater

NO production in a staged combustor and diminishing the suitability of humidification for NO_x reduction.

A database of analytical results was generated, useful to the community for CFD validation, as increased work is undertaken with NH_3 flames.

ACKNOWLEDGEMENTS

This work was supported by the FLEXIS project with funding from the Welsh European Funding Office. The research was undertaken at the Cardiff University's Gas Turbine Research Centre with invaluable technical support from Jack Thomas.

REFERENCES

[1] Valera-Medina, Agustin, Xiao, Hua, Owen-Jones, Martin, David, William, Bowen, Philip "Ammonia for power.", Progress in Energy and combustion science Vol 69 (2018): 63-102. https://doi.org/10.1016/j.pecs.2018.07.001

[2] Kobayashi, Hideaki, Hayakawa, Akihiro. Somarathne K.D. Kunkuma A, and Okafor, Ekenechukwu C. "Science and technology of ammonia combustion", Proceedings of the combustion institute Vol 37 (2019): 109-133. https://doi.org/10.1016/j.proci.2018.09.029

[3] Pugh, Daniel, Bowen Philip, Valera-Medina, Agustin, Giles, Anthony, Runyon, Jon and Marsh, Richard "Influence of steam addition and elevated ambient conditions on NOx reduction in a staged premixed swirling NH_3/H_2 flame", Proceedings of the combustion institute Vol 37 (4) (2019): 5401-5409 https://doi.org/10.1016/j.proci.2018.07.091

[4] Pfahl, U.J. Ross, M.C. Shepherd J.E., Pasamehmetoglu K.O. and Unal, C. "Flammability limits, ignition energy, and flame speeds in H_2–CH_4–NH_3–N_2O–O_2–N_2 mixtures", Combustion and flame Vol 123 (2000): 140-158. https://doi.org/10.1016/S0010-2180(00)00152-8

[5] Daniel. Pugh, et al. "An Investigation of Ammonia Primary Flame Combustor Concepts for Emissions Reduction with OH*, NH_2* and NH*Chemiluminescence at Elevated Conditions", Proc. Comb. Inst. (2020) under review.

[6] Mathieu, Oliver, and Petersen, Eric "Experimental and modeling study on the high-temperature oxidation of Ammonia and related NO_x chemistry", Combustion and flame Vol 162 (2015): 554-570 https://doi.org/10.1016/j.combustflame.2014.08.022

[7] Nozari, Hadi, Karaca, Gizen, Tuncer, Onur, and Karabeyoglu, Arif "Porous medium based burner for efficient and clean combustion of ammonia–hydrogen–air systems", International Journal of Hydrogen Energy Vol 42 (21) (2017): 14775-14785 https://doi.org/10.1016/j.ijhydene.2017.03.234

[8] Guteša Božo, Vigueras-Zuniga, Buffi, Marco, Seljak, T. and Valera-Medina, Agustin "Fuel rich ammonia-hydrogen injection for humidified gas turbines", Applied Energy Vol 251 (2019): 113334. https://doi.org/10.1016/j.apenergy.2019.113334

[9] Valera-Medina, Agustin, Pugh, Daniel, Marsh, Richard, Bulat, G. and Bowen, Philip "Preliminary study on lean premixed combustion of ammonia-hydrogen for swirling gas turbine combustors" International Journal of Hydrogen Energy Vol 42 (2017): 24495-24503. https://doi.org/10.1016/j.ijhydene.2017.08.028

[10] Kurata, Osamu, Iki, Norihiko Matsunuma, Takayuki, Inoue, Takahiro and Hayakawa Akihiro "Performances and emission characteristics of NH_3–air and NH_3–CH_4–air combustion gas-turbine power generations" Proceedings of the combustion institute Vol 36 (3) (2017): 3351-3359 https://doi.org/10.1016/j.proci.2016.07.088

[11] Okafor, Ekenechukwu C. Naito, Yuji, Colson, Sophie, Ichikawa, Akinori, Kudo, Taku, Hayakawa Akihiro and Kobayashi Hideaki "Experimental and numerical study of the laminar burning velocity of CH_4–NH_3–air premixed flames", Combustion and flame Vol 187 (2018): 185-198 https://doi.org/10.1016/j.combustflame.2017.09.002

[12] Valera-Medina, Agustin, Marsh Richard,, Runyon, Jon, Pugh, Daniel, Beasley, Paul, , Hughes, Timothy and Bowen, Philip, "Ammonia–methane combustion in tangential swirl burners for gas turbine power generation", Applied Energy Vol 185 (2) (2017): 1362-1371 https://doi.org/10.1016/j.apenergy.2016.02.073

[13] Hayakawa, Akihiro, Arakawa, Yoshiyuki, Mimoto, Rentaro, A. Somarathne, K.D. Kunkuma, Kudo, Taku, and Kobayashi, Hideaki, "Experimental investigation of stabilization and emission characteristics of ammonia/air premixed flames in a swirl combustor", International Journal of Hydrogen Energy Vol 42 (19) (2017): 14010-14018. https://doi.org/10.1016/j.ijhydene.2017.01.046

[14] Kurata Osamu,, Iki, Norihiko, Inoue, Takahiro, Matsunuma, Takayuki, Tsujimura, Taku, Furutani, Hirohide, Kawano, Masato, Araic, Keisuke, Okafor, Ekenechukwu C. Hayakawa, Akihiro, and Kobayashi Hideaki, "Development of a wide range-operable, rich-lean low-NOx combustor for NH_3 fuel gas-turbine power generation", Proceedings of the combustion institute Vol 37 (4) (2019): 4587-4595. https://doi.org/10.1016/j.proci.2018.09.012

[15] Somarathne, Kapuruge Don Kunkuma Amila, Okafor, Ekenechukwu C. Hayakawa, Akihiro Taku ,Kudo Kurata, Osamu, Norihiko, Iki and Hideaki, Kobayashi "Emission characteristics of turbulent non-premixed ammonia/air and methane/air swirl flames through a rich-lean combustor under various wall thermal boundary conditions at high pressure", Combustion and flame Vol 210 (2019): 247-261. https://doi.org/10.1016/j.combustflame.2019.08.037

[16] Somarathne, Kapuruge Don Kunkuma Amila, Hatakeyama, Sotaro, Hayakawa, Akihiro and Kobayashi, Hideaki, "Numerical study of a low emission gas turbine like combustor for turbulent ammonia/air premixed swirl flames with a secondary air injection at high pressure" International Journal of Hydrogen Energy Vol 42 (44) (2017) 27388-27399. https://doi.org/10.1016/j.ijhydene.2017.09.089

[17] Okafor, Ekenechukwu C. Somarathne, Kapuruge Don Kunkuma Amila, Hayakawa, Akihiro, Taku ,Kudo Kurata, Osamu, Norihiko, Iki and Hideaki, Kobayashi "Towards the development of an efficient low-NOx ammonia combustor for a micro gas turbine", Proceedings of the combustion institute Vol 37 (4) (2019): 4597-4606.
https://doi.org/10.1016/j.proci.2018.07.083

[18] Okafor, Ekenechukwu C. Somarathne, Kapuruge Don Kunkuma Amila, Ratthanan, Rattanasupapornsak, Hayakawa, Akihiro, Taku, Kudo, Kurata, Osamu, Norihiko, Iki, Tsujimur, Taku, Furutani, Hirohide and Kobayashi Hideaki, "Control of NO_x and other emissions in micro gas turbine combustors fuelled with mixtures of methane and ammonia", Combustion and flame Vol 211 (2020): 406-416.
https://doi.org/10.1016/j.combustflame.2019.10.012

[19] Pugh, Daniel, Bowen Philip, Marsh, Richard, Crayford, Andrew, Runyon, Jon Morris, Steven, Valera-Medina, Agustin Agustin, and Giles, Anthony, "Dissociative influence of H_2O vapour/spray on lean blowoff and NOx reduction for heavily carbonaceous syngas swirling flames", Combustion and flame Vol 177 (2017): 37-48.
https://doi.org/10.1016/j.combustflame.2016.11.010

[20] Pugh, Daniel, Bowen Philip, Crayford, Andrew, Marsh, Richard, Runyon, Jon Morris, Steven, and Giles, Anthony, "Catalytic Influence of Water Vapor on Lean Blow-Off and NOx Reduction for Pressurized Swirling Syngas Flames", Journal of Engineering for Gas Turbines and Power Vol 140 (6) (2018): 2018, 061502.
https://doi.org/10.1115/1.4038417

[21] British Standard ISO 11042-1:1996, Gas turbines. Exhaust gas emission Measurement and evaluation, British Standards Institution, U.K. (1996).

[22] Runyon, Jon, Giles, Anthony, Marsh, Richard, Pugh, Daniel, Goktepe, Burak Bowen, Philip and Morris, Steven, "Characterization of ALM Swirl Burner Surface Roughness and Its Effects on Flame Stability Using High-speed Diagnostics" Journal of Engineering for Gas Turbines and Power Vol 142(4) (2020): 041017 https://doi.org/10.1115/1.4044950

[23] A. G. Gaydon, "The Spectroscopy of Flames", 2nd Edition. Chapman and Hall. London U.K. 1974.

[24] Fontijn, A. "Mechanism of CN and NH Chemiluminescence in the $N–O–C_2H_2$ and $O–NO–C_2H_2$ Reactions" Journal of Chemical Physics Vol 43, (1965):
https://doi.org/10.1063/1.1697018

[25] Bergeat, A. Calvo, T. Daugey, N. Loison, J-C, and Dorthe. G. "Product Branching Ratios of the CH + NO Reaction," Journal of Chemical Physics Vol. 102 (42) (1998): 8124-8130. https://doi.org/10.1021/jp9820929

[26] Yi, Yanhui, Zhang, Rui, Wang, Li, Yan, Jinhui,Zhang, Jialiang, Guo, and Hongchen, "Plasma-Triggered CH_4/NH_3 Coupling Reaction for Direct Synthesis of Liquid Nitrogen-Containing Organic Chemicals", ACS Omega, 2 (12) (2017): 9199-9210 https://doi.org/10.1021/acsomega.7b01060

[27] Ohashi Kazuhiko, Kasai, Toshio, , Chil Che, Dock and Kuwata, Keiji, "Alignment dependence of the amidogen chemiluminescence in the reaction of argon(3P) atoms with the aligned ammonia molecules", Journal of Chemical Physics Vol. 93 (14) (1989) 5484-5487 https://doi.org/10.1021/j100351a033

[28] Schott, Garry L. Blair, Larry S. and Morgan, John D. "Exploratory shock-wave study of thermal nitrogen trifluoride decomposition and reactions of nitrogen trifluoride and dinitrogen tetrafluoride with hydrogen" Journal of Chemical Physics Vol. 77 (24) (1973): 2823-2830
https://doi.org/10.1021/j100642a001

[29]. Roose T.R, Hanson, R.K. and Kruger C.H., "A shock tube study of the decomposition of no in the presence of NH_3", Proceedings of the combustion institute Vol 18 (1) (1981): 853-862. https://doi.org/10.1016/S0082-0784(81)80089-6

[30] Bowman, C., Frenklach, M., Gardiner, W., and Smith, G., 1999, "The 'GRIMech 3.0' Chemical Kinetic Mechanism," University of California Berkeley, Berkeley, CA, (2015)

[31] Runyon, Jon, Marsh, Richard, Bowen, Philip, Pugh, Daniel, Giles, Anthony, and Morris, Steven, "Lean methane flame stability in a premixed generic swirl burner: Isothermal flow and atmospheric combustion characterization", Experimental Thermal and Fluid Science Vol 92 (2018): 125-140. https://doi.org/10.1016/j.expthermflusci.2017.11.019

[32] Peterson, Christopher, Sowa, William, and Samuelsen, G.S. "Performance of a model rich burn-quick mix-lean burn combustor at elevated temperature and pressure", NASA/CR-2002-211992.